Supporting Information for

Violation or Abidance of Löwenstein's Rule in Zeolites Under Synthesis Conditions?

Xiaomin Tang,[†,∥,⊥] Zhiqiang Liu,[†,⊥] Ling Huang,[†] Wei Chen,[†] Chengbin Li,[†] Guiru Wang,[†] Guangchao Li,[†,∥] Xianfeng Yi,[†] Anmin Zheng*[,†,‡,§]

[†]State Key Laboratory of Magnetic Resonance and Atomic and Molecular Physics, National Center for Magnetic Resonance in Wuhan, Key Laboratory of Magnetic Resonance in Biological Systems, Wuhan Institute of Physics and Mathematics, Innovation Academy for Precision Measurement Science and Technology, Chinese Academy of Sciences, Wuhan 430071, P.R. China

[‡]Wuhan National Laboratory for Optoelectronics, Huazhong University of Science and Technology, Wuhan 430074, P.R. China

[§]School of Materials Science and Engineering, Zhengzhou University, Zhengzhou, Henan 450001, P.R. China

[∥]University of Chinese Academy of Sciences, Beijing 100049, P.R. China

E-mail: zhenganm@wipm.ac.cn

S1. Computational details

All framework structures (CHA and MOR) with all-silica form were obtained from the Database of Zeolite Structures. [1] For H-zeolites, the global minima L and NL structures of H-SSZ-13 with Si/Al = 17, as well as the global minima NL structure of H-SSZ-13 with Si/Al = 11 were referred to Fletcher's work. [2] Schematic illustrations of structures used in this work were drawn using the program VESTA 3 [3] and VMD. [4]

All the calculations, including the periodic density functional theory (DFT) calculations, vibrational modes calculations and *ab initio* molecular dynamics (AIMD) simulations, were performed using the CP2K code. [5-7] In our calculations, the Perdew-Burke-Ernzerhof (PBE) exchange-correlation functional [8] was applied and the D3 correction [9] of Grimme was used due to the importance of van der Waals interaction between SDA and zeolites. [10] During the optimization, all structures were relaxed for CHA ($1 \times 1 \times 1$) and MOR ($1 \times 1 \times 2$) by using the TZV2P basis set and GTH pseudo potentials. [11] The plane wave cutoff energy and relative cutoff was 650 Ry and 60 Ry, respectively. For the calculation of vibrational modes, the finite differences method was employed, with 0.01 Å displacement.

The Gibbs free energy was calculated according to Resasco's work. [12] It is noteworthy that the used harmonic approximation can roughly estimate of the entropy. Small imaginary modes with frequencies lower than 100 cm^{-1} were not involved in the Gibbs free energy calculation. [13-14] Additionally, a 30 ps AIMD simulation was performed in the NVT ensemble using the Nosé-Hoover thermostat [15] with a time step of 0.5 fs for CHA framework at 433 K. The first 5 ps AIMD simulation was used for equilibration while the remaining 25 ps for calculating the directing probability (P(O) and P(T)). The energy cutoff and relative cutoff was also 650 Ry and 60 Ry, respectively. The DZVP basis set with GTH pseudo potentials have been chosen for all the elements during the 30 ps AIMD process.

S2. Check for the reliability of the theoretical method used in our work.

The global minima L and NL H-SSZ-13 structures with Si/Al = 17 have been proposed in Fletcher's work, [2] and a brief confirmation is carried out in our work. The L and NL frameworks are adopted but with each proton residing at one of four O atoms bonded to Al atom. There are four distinct O atoms (O_1, O_2, O_3 and O_4) linked to each T atom in CHA-type zeolites (SSZ-13). O_i-O_j (i = 1-4, j = 1-4) in Table S1 represents that one proton resides at O_i atom bonded to Al_1, while the other proton resides at O_j atom bonded to Al_2. It should be pointed out that the proton distribution of O_1-O_1 for NL configuration is abandoned, because the two protons are unreasonably residing at the same O atom. According to the relative energy of L and NL structures with various proton distributions shown in Table S1, the configurations which correspond to the underlined values in bold are the most stable NL structure (0 kJ/mol used as the reference, Figure S2b) and L structure (Figure S2a), respectively.

Table S1. Relative energy of L and NL H-SSZ-13 zeolites with various proton distributions.

proton distribution	Relative energy (kJ/mol)	
	L	NL
O_1-O_1	41.1	---
O_1-O_2	45.5	22.7
O_1-O_3	16.8	15.5
O_1-O_4	71.7	**<u>0.0</u>**
O_2-O_1	58.8	22.0
O_2-O_2	66.9	91.2
O_2-O_3	40.6	85.1
O_2-O_4	50.3	77.6
O_3-O_1	54.9	15.7
O_3-O_2	60.0	85.1
O_3-O_3	40.2	78.8
O_3-O_4	34.6	68.5
O_4-O_1	43.1	0.2
O_4-O_2	45.2	77.6
O_4-O_3	74.7	69.3
O_4-O_4	**<u>14.7</u>**	75.8

From the results listed in Table S1 and configurations in Figure S2, we could see that the H locations of the global minima L and NL structures are consistent with that in Fletcher's work, [2] and the energy difference between the most stable L and NL structures is 14.7 kJ/mol, which is in good agreement with 14.2 kJ/mol in Fletcher's work. Therefore, there is no need to repeat the calculation of all optimizations of H-zeolites because Fletcher *et al.* have done it systematically, and the H-zeolites structures could be adopted in our work directly.

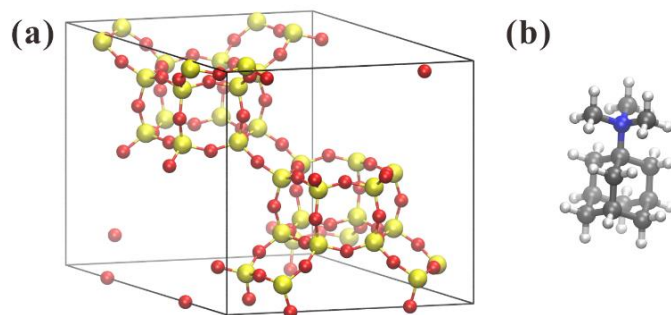## S3. Structures of SSZ-13 zeolite and TMAda$^+$ cation.

Figure S1. Structures of (a) SSZ-13 zeolite and (b) organic structure-directing agent (SDA) of N,N,N-trimethyl-1-adamantammonium cation (TMAda$^+$) used for the synthesis of SSZ-13 zeolite. [16-20] Si atoms are shown in yellow, O are shown in red, N are shown in blue, C are shown in gray, and H are shown in white.

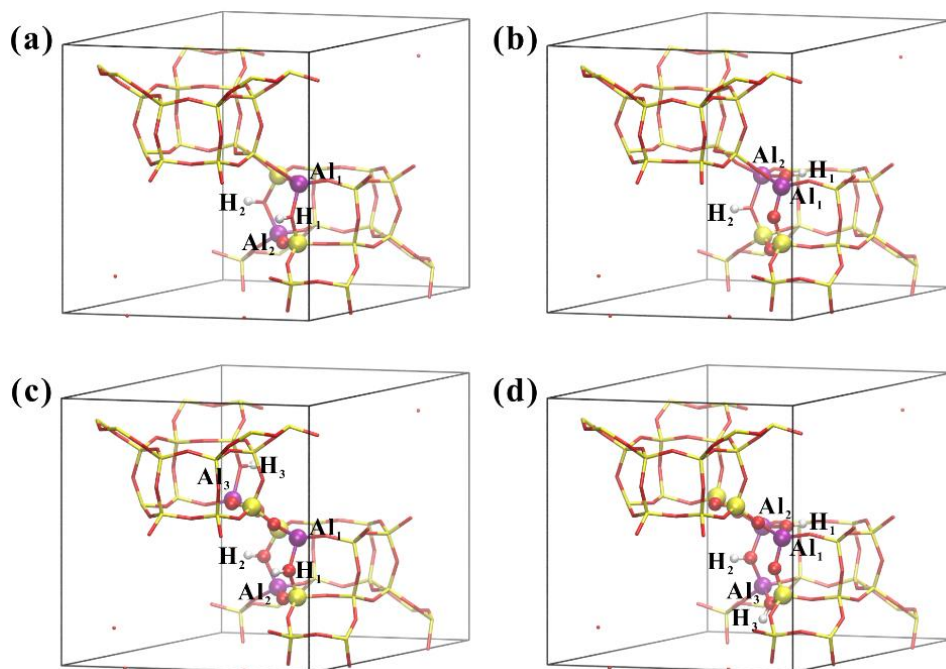**S4. Optimized structures of H-SSZ-13 zeolites according to DFT calculation.**

Figure S2. (a) L and (b) NL structure of H-SSZ-13 with 2 Al per unit cell (Si/Al = 17); (c) L and (d) NL structure of H-SSZ-13 with 3 Al per unit cell (Si/Al = 11). Si atoms are shown in yellow, Al are shown in purple, O are shown in red, and H are shown in white.

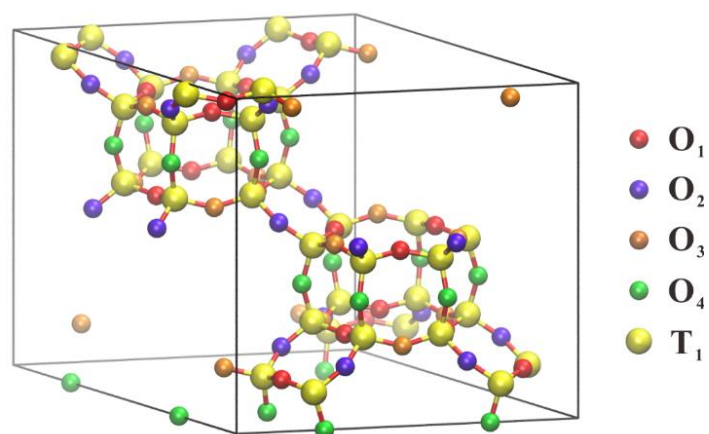**S5. Crystal structure of SSZ-13 zeolite.**

Figure S3. Crystal structure of SSZ-13 zeolite with CHA-type framework topology, which contains one crystallographic equivalent T site and four O sites corresponding to O_1, O_2, O_3 and O_4, respectively.

S6. Optimized structures of SDA-zeolite complexes according to DFT calculation.

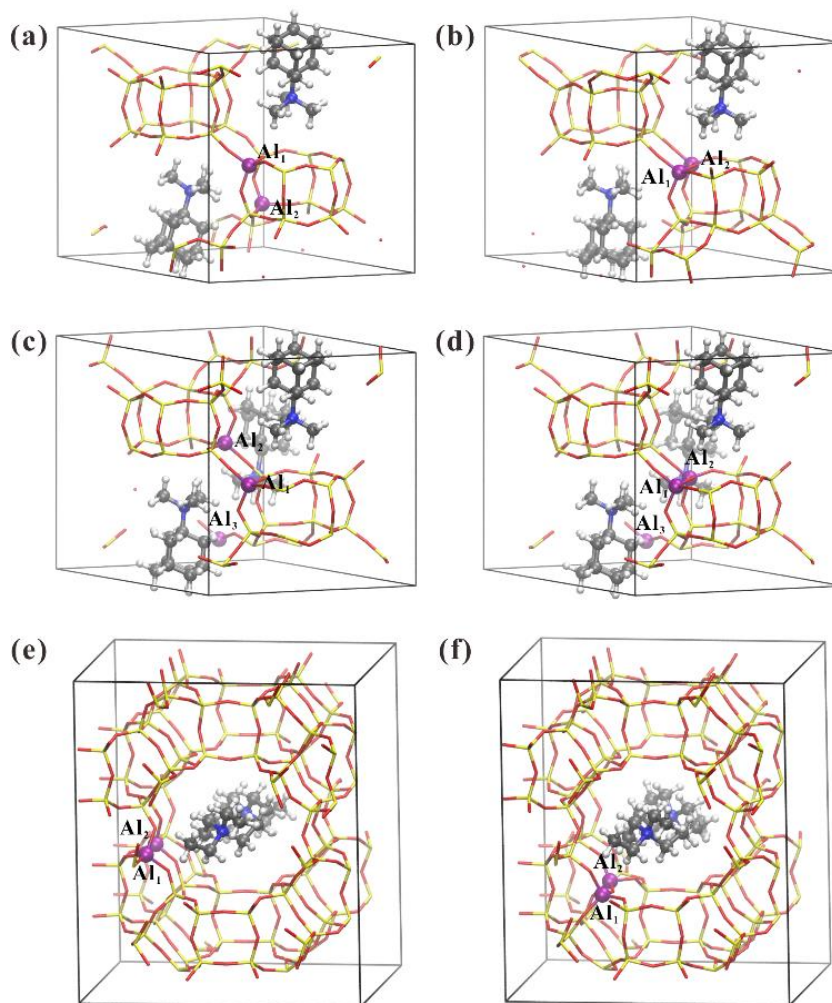Figure S4. (a) L and (b) NL structure of SDA-SSZ-13 complex with 2 TMAda$^+$ per unit cell (Si/Al = 17); (c) L and (d) NL structure of SDA-SSZ-13 complex with 3 TMAda$^+$ per unit cell (Si/Al = 11); (e) L and (f) NL structure of SDA-MOR complex with 2 TEA$^+$ (Si/Al = 47). Si atoms are shown in yellow, Al are shown in purple, O are shown in red, N are shown in blue, C are shown in gray, and H are shown in white.

S7. Check for the applicability of Löwenstein's rule in MOR framework.

To check whether the applicability of the preference for L over NL configuration can be extended to other zeolites, MOR frameworks trapped with tetraethylammonium cations (TEA$^+$, a typical SDA for MOR synthesis) have been investigated as well. The MOR framework possesses 4 symmetry distinct T sites, and all the possible combinations of Al distribution (*i.e.*, T_1-O_1-T_1, T_1-O_2-T_1, T_1-O_4-T_2, T_1-O_3-T_3, T_2-O_5-T_2, T_2-O_6-T_2, T_2-O_7-T_4, T_3-O_8-T_3, T_3-O_9-T_4, and T_4-O_{10}-T_4. But the T_3 site is inaccessible to TEA$^+$ and hence combinations including T_3 site are excluded) for NL SDA-MOR complexes are considered. It has been demonstrated that the NL structure is more stable than the L structure for H-MOR by Fletcher and co-workers. However, with SDA (TEA$^+$) trapped inside the MOR framework, the L structure is more stable than the NL configuration with a ΔE_{NL-L} of 41.3 kJ/mol. Apparently, it is indicative that Löwenstein's rule is still obeyed in MOR framework with the presence of SDA.
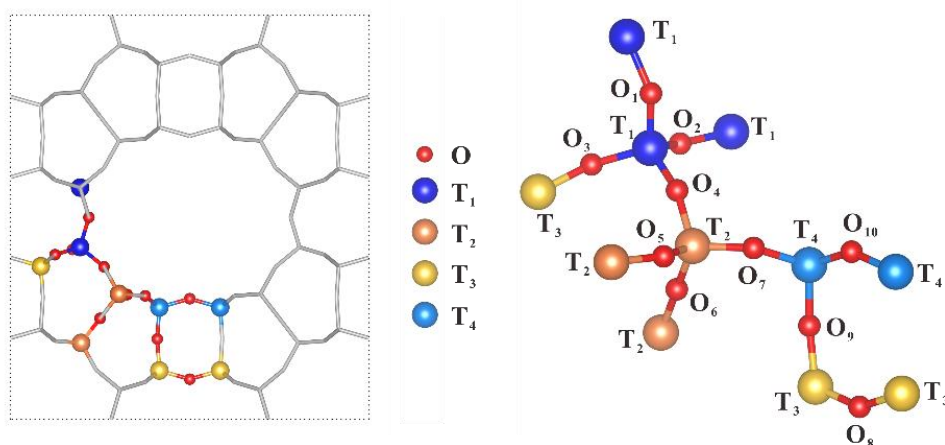
Figure S5. The MOR framework as well as labeled T and O sites.

S8. The most two stable paired Al configurations.

Figure S6. (a) The most stable paired Al configuration (-Al-(O-Si)$_2$-O-Al-) with Na$^+$ located at SI site. (b) The next-stable paired Al configuration (-Al-O-Si-O-Al-) with Na$^+$ located at SI site. Si atoms are shown in yellow, Al are shown in purple, O are shown in red, N are shown in blue, C are shown in gray, H are shown in white, and Na are shown in cyanine.

S9. Method for generating water adsorption configurations.

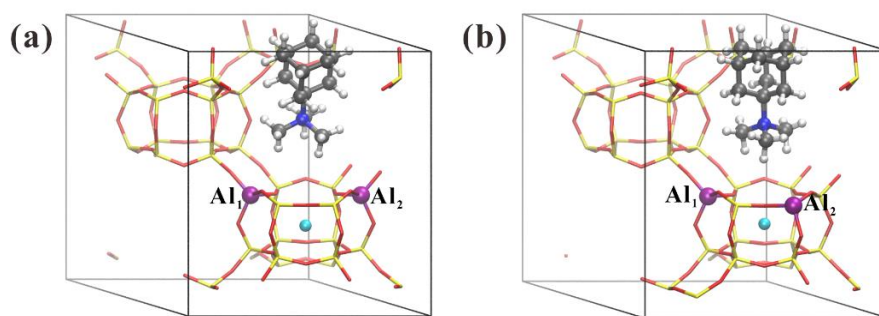First of all, Grand Canonical Monte Carlo simulation is performed to obtain the saturated loading of water molecules for SDA-SSZ-13 complexes under synthesis temperature (433 K). In the grand canonical ensemble (μVT), the chemical potential, volume and temperature are fixed. Metropolis method [21] is employed while coarse calculation quality is set. The calculations are carried out in 2×10^7 Monte Carlo (MC) steps where the first 1×10^7 steps are used for equilibration, and the rest 1×10^7 steps for statistical averaging. During the MC simulations, four trial moves of molecules are randomly attempted: displacement, rotation, translation and regrowth with probabilities of 50%, 24%, 24% and 2% are used, respectively. The consistent valence force field (CVFF) force field, [22] which is a generalized valence force field and could describe the interaction of water/SDA/zeolites well, [23, 24] is used in our work. The loading of water molecules is 6 per unit cell for SDA-SSZ-13 complex with Si/Al = 11 and 21 per unit cell for SDA-SSZ-13 complex with Si/Al = 17, respectively. The adsorption configurations for water molecules are derived from MC simulations in the canonical ensemble (NVT). And five different initial structures are obtained from an anneal process for each case of Al distribution (*i.e.*, the L and NL (Al$_1$-O$_x$-Al$_2$, x = 1, 2, 3, 4) structures with Si/Al = 17, L and the most stable NL structures with Si/Al = 11) to investigate the influence of water on Al distribution. The most stable configurations are used to be analyzed. The MC simulations are performed with Sorption module and the anneal simulation is performed with Forcite module in the Material Studio 7.0. [25] All the theoretical simulations in this section are completed in National Supercomputing Center in Shenzhen (NSCS) and SINOPEC.

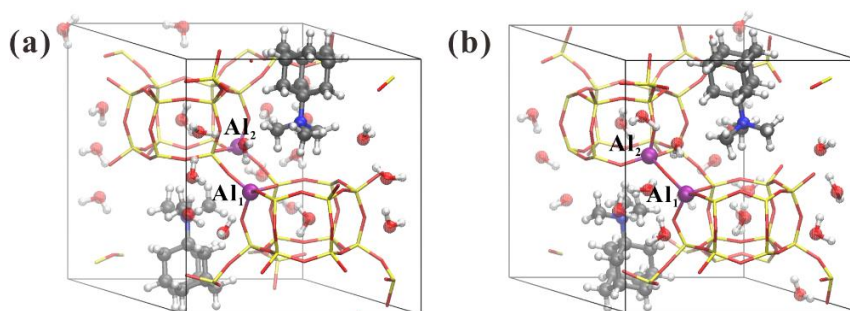**S10. Newly predicted SSZ-13 zeolite structures.**

Figure S7. Newly predicted structures of (a) L_1 and (b) NL_1 SDA-SSZ-13 complexes on the basis of the directing probabilities (P(T)). Si atoms are shown in yellow, Al are shown in purple, O are shown in red, N are shown in blue, C are shown in gray, and H are shown in white.

S11. The acidic proton distribution in the newly predicted L SSZ-13 zeolite.

After the determination of the Al distribution of the new L SSZ-13 structure (Figure S7a), the acidic proton distribution is further investigated by DFT calculation. For H-SSZ-13, each proton may reside at one of the four O atoms which are linked to Al atom. Therefore, a total of 16 configurations with different proton distributions have been generated. Table S2 presents the relative energy of the new L SSZ-13 zeolite with various proton distributions.

Table S2. Relative energy of the new L SSZ-13 zeolite with various proton distributions.

proton distribution	Relative energy (kJ/mol)
O_1-O_1	**0.0**
O_1-O_2	82.2
O_1-O_3	34.7
O_1-O_4	27.8
O_2-O_1	82.8
O_2-O_2	21.1
O_2-O_3	35.3
O_2-O_4	43.7
O_3-O_1	35.4
O_3-O_2	34.1
O_3-O_3	54.2
O_3-O_4	44.6
O_4-O_1	28.9
O_4-O_2	44.0
O_4-O_3	45.9
O_4-O_4	42.3

According to the relative energy of the new L H-SSZ-13 zeolite with various proton distributions (Table S2), the configuration which corresponds to the underlined value in bold is the most stable structure (0 kJ/mol used as the reference, Figure S8). The protons are both directed into the plane of 6-MR in the most stable H-SSZ-13 structure.
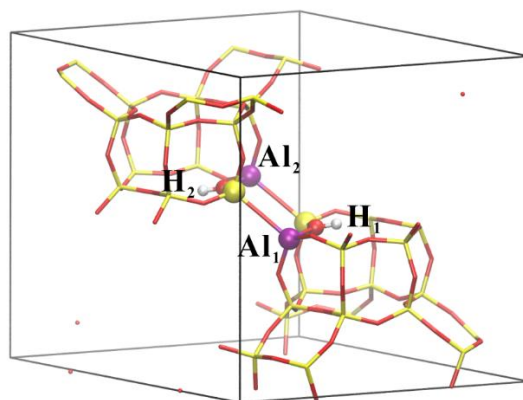
Figure S8. The most stable new L H-SSZ-13 with 2 Al per unit cell (Si/Al = 17). Si atoms are shown in yellow, Al are shown in purple, O are shown in red, and H are shown in white.

S12. The flow diagram for predicting new structures with more preferred Al distribution.

The computational flow diagram for predicting new structures with more preferred Al distribution is shown in Figure S9 and presented here.

1. The *ab initio* molecular dynamics (AIMD) simulation was performed to get the trajectory of the SDA-zeolite complex under solvation conditions (initial structure).

2. Do statistics of the probability of the framework O atoms ($P(O)$) being the closest to the N atom in SDA. The probability of the ith O atom ($P(O_i)$) was calculated according to the following equation:

$$P(O_i) = \frac{N(O_i)}{\sum_i N(O_i)} \tag{1}$$

where $N(O_i)$ represents the count of the ith O atom being the nearest to the N atom in SDA during the AIMD simulation. $\sum_i N(O_i)$ represents the total count over all the O atoms in the zeolite framework.

3. Do statistics of the probability of SDA directing Al atom to the jth T atom ($P(T_j)$, T = Si or Al) according to the following equation:

$$P(T_j) = \frac{1}{2} \sum_{i=1}^{4} P(O_{ji}) \tag{2}$$

where O_{ji} (i = 1, 2, 3, 4) corresponds to the four neighbored O_i atoms which are bonded to T_j atom. 1/2 represents that $P(O)$ contributes equally to two $P(T)$ (one O atom connects with two T atoms).

4. Generate the new structure by substituting the T_j position which owns the maximum probability ($P(T_j)$) with Al atom and other positions with Si atom. If there are more than one SDA in the zeolite framework, repeat steps 2, 3 and 4 until all Al atoms have been substituted (assume the number of Al and SDA is the same). It should be pointed out that T_j which has been substituted by Al atom did not change in subsequent cycles.

5. Optimize the new structure by DFT calculation and compare the relative energy between the new configuration and initial structure. If the energy of the new structure

is higher than the initial one, then reset the initial structure by using the new structure

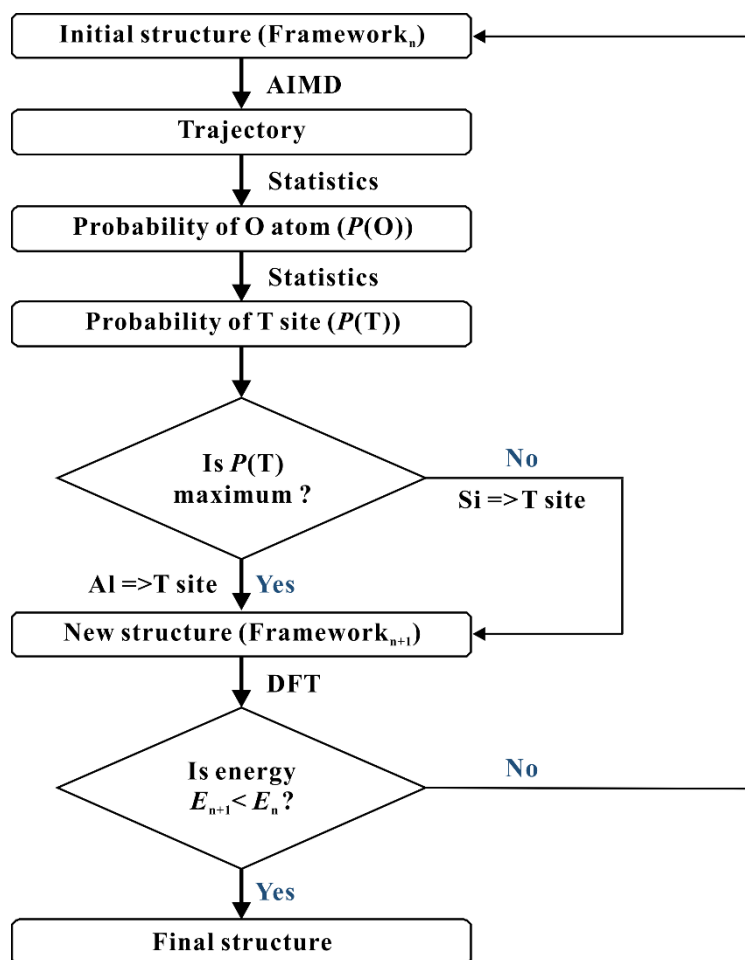and go to step 1, otherwise, the new structure is exported as the final structure.

Figure S9. Flow diagram showing the procedure for predicting new structure.

S13. The directing function of SDA in NL structure.

For the NL configuration as the initial structure, the preferred T atom (T = Si or Al) positions where SDA_1 directed are mainly located in Si_1 (45.4%), thus Si_1 position seems to be the preferential Al location (Figure S10a). While the preferred T positions where SDA_2 directed are relatively more dispersed, the probability of Si_2 (23.0%) is higher than that of other T atoms, thus Si_2 position seems to be more suitable for Al location (Figure S10b). As a consequence, the combination of Si_1 and Si_2 positions substituted by Al atoms leads to the new L configuration (L_2, Figure S11). And this new L_2 structure is 10.1 kJ/mol more stable than the NL structure. In conclusion, the L structure is more preferred than the NL configuration, once again indicating the validity of Löwenstein's rule.
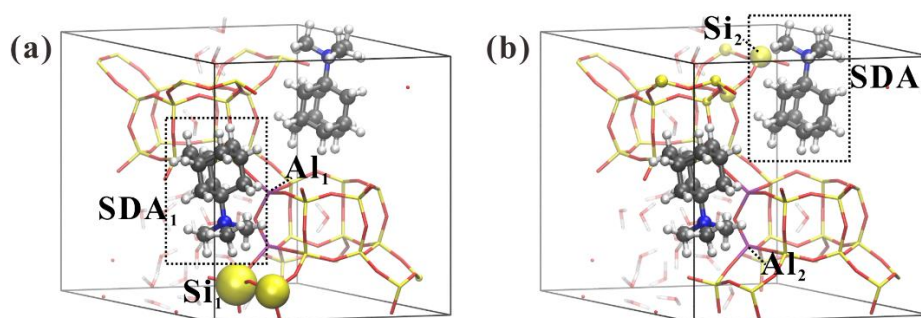
Figure S10. Probability of (a) SDA_1, (b) SDA_2 for directing Al atom into specific T sites (P(T)) in the NL conformation. The size of yellow and purple spheres is scaled to P(T). Si atoms are shown in yellow, Al are shown in purple, O are shown in red, N are shown in blue, C are shown in gray, and H are shown in white.

Figure S11. Newly predicted structure of L SDA-SSZ-13 complex (L_2) on the basis of the directing probabilities (P(T)). Si atoms are shown in yellow, Al are shown in purple, O are shown in red, N are shown in blue, C are shown in gray, and H are shown in white.

References

1.   Baerlocher, C.; McCusker, L. B. Database of Zeolite Structures. http://www.iza-structure.org/databases/ (Accessed Jun 2016).
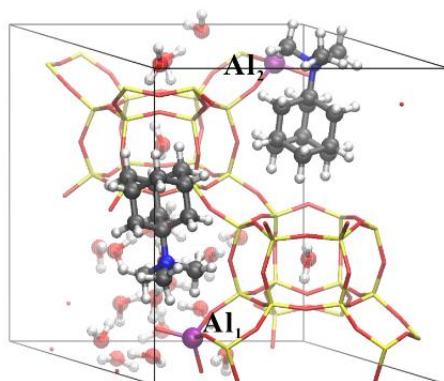
2.   Fletcher, R. E.; Ling, S. L.; Slater, B. Violations of Lowenstein's Rule in Zeolites. *Chem. Sci.* **2017,** *8*, 7483-7491.

3.   Momma, K.; Izumi, F. VESTA 3 for Three-Dimensional Visualization of Crystal, Volumetric and Morphology Data. *J. Appl. Crystallogr.* **2011,** *44*, 1272-1276.

4.   Humphrey, W.; Dalke, A.; Schulten, K. VMD: Visual Molecular Dynamics. *J. Mol. Graphics* **1996,** *14*, 33-38.

5.   Available at: https://www.cp2k.org/.

6.   VandeVondele, J.; Krack, M.; Mohamed, F.; Parrinello, M.; Chassaing, T.; Hutter, J. QUICKSTEP: Fast and Accurate Density Functional Calculations Using a Mixed Gaussian and Plane Waves Approach. *Comput. Phys. Commun.* **2005,** *167*, 103-128.

7.   VandeVondele, J.; Hutter, J. Gaussian Basis Sets for Accurate Calculations on Molecular Systems in Gas and Condensed Phases. *J. Chem. Phys.* **2007,** *127*, 114105.

8.   Perdew, J. P.; Burke, K.; Ernzerhof, M. Generalized Gradient Approximation Made Simple (vol 77, pg 3865, 1996). *Phys. Rev. Lett.* **1997,** *78*, 1396-1396.

9.   Grimme, S.; Antony, J.; Ehrlich, S.; Krieg, H. A Consistent and Accurate Ab Initio Parametrization of Density Functional Dispersion Correction (DFT-D) for the 94 Elements H-Pu. *J. Chem. Phys.* **2010,** *132,* 154104.

10. Sanchez, M.; Diaz, R. D.; Cordova, T.; Gonzalez, G.; Ruette, F. Study of Template Interactions in MFI and MEL Zeolites Using Quantum Methods. *Micropor. Mesopor. Mater.* **2015,** *203*, 91-99.

11. Goedecker, S.; Teter, M.; Hutter, J. Separable Dual-Space Gaussian Pseudopotentials. *Phys. Rev. B* **1996,** *54*, 1703-1710.

12. Zhao, Z.; Bababrik, R.; Xue, W. H.; Li, Y. P.; Briggs, N. M.; Nguyen, D. T.; Nguyen, U.; Crossley, S. P.; Wang, S. W.; Wang, B.; Resasco, D. E. Solvent-Mediated Charge Separation Drives Alternative Hydrogenation Path of Furanics in Liquid Water. *Nat. Catal.* **2019,** *2*, 431-436.

13. Gunst, D.; Alexopoulos, K.; Van der Borght, K.; John, M.; Galvita, V.; Reyniers, M. F.; Verberckmoes, A. Study of Butanol Conversion to Butenes over H-ZSM-5: Effect of Chemical Structure on Activity, Selectivity and Reaction Pathways. *Appl. Catal. A Gen.* **2017,** *539*, 1-12.

14. Boronat, M.; Viruela, P. M.; Corma, A. Reaction Intermediates in Acid Catalysis by Zeolites: Prediction of the Relative Tendency to Form Alkoxides or Carbocations as a Function of Hydrocarbon Nature and Active Site Structure. *J. Am. Chem. Soc.* **2004,** *126*, 3300-3309.

15. Tuckerman, M. E.; Liu, Y.; Ciccotti, G.; Martyna, G. J. Non-Hamiltonian Molecular Dynamics: Generalizing Hamiltonian Phase Space Principles to Non-Hamiltonian Systems. *J. Chem. Phys.* **2001,** *115*, 1678-1702.

16. Di Iorio, J. R.; Gounder, R. Controlling the Isolation and Pairing of Aluminum in Chabazite Zeolites Using Mixtures of Organic and Inorganic Structure-Directing Agents. *Chem. Mater.* **2016,** *28*, 2236-2247.

17. Wu, L. L.; Degirmenci, V.; Magusin, P. C. M. M.; Szyja, B. M.; Hensen, E. J. M. Dual Template Synthesis of a Highly Mesoporous SSZ-13 Zeolite with Improved Stability in the Methanol-To-Olefins Reaction. *Chem. Commun.* **2012,** *48*, 9492-9494.

18. Martinez-Franco, R.; Moliner, M.; Thogersen, J. R.; Corma, A. Efficient One-Pot Preparation of Cu-SSZ-13 Materials Using Cooperative OSDAs for Their Catalytic Application in the SCR of NOx. *ChemCatChem* **2013,** *5*, 3316-3323.

19. Kumar, M.; Luo, H.; Roman-Leshkov, Y.; Rimer, J. D. SSZ-13 Crystallization by Particle Attachment and Deterministic Pathways to Crystal Size Control. *J. Am. Chem. Soc.* **2015,** *137*, 13007-13017.

20. Xu, R. N.; Zhang, R. D.; Liu, N.; Chen, B. H.; Qiao, S. Z. Template Design and Economical Strategy for the Synthesis of SSZ-13 (CHA-Type) Zeolite as an Excellent Catalyst for the Selective Catalytic Reduction of NOx by Ammonia. *ChemCatChem* **2015,** *7*, 3842-3847.

21. Metropolis, N.; Rosenbluth, A. W.; Rosenbluth, M. N.; Teller, A. H.; Teller, E. Equation of State Calculations by Fast Computing Machines. *J. Chem. Phys.* **1953,** *21*,

1087-1092.

22. Dauberosguthorpe, P.; Roberts, V. A.; Osguthorpe, D. J.; Wolff, J.; Genest, M.; Hagler, A. T. Structure and Energetics of Ligand-Binding to Proteins - Escherichia-Coli Dihydrofolate Reductase Trimethoprim, a Drug-Receptor System. *Proteins* **1988,** *4*, 31-47.

23. Pinar, A. B.; Gomez-Hortiguela, L.; McCusker, L. B.; Perez-Pariente, J. Controlling the Aluminum Distribution in the Zeolite Ferrierite via the Organic Structure Directing Agent. *Chem. Mater* **2013,** *25*, 3654-3661.

24. Szyja, B.; Jansen, A.; Verstraelen, T.; van Santen, R. Molecular Dynamics Study of the Silica-Water-SDA Interactions. *Phys. Chem. Chem. Phys.* **2009,** *11*, 7605-7610.

25. Materials Studio v 7.0. Accelrys Software Inc., San Diego, CA 92121, USA.